CrystEngComm

X-ray diffraction study on the orientation dynamics of biaxial microcrystals under static and rotating magnetic fields

Journal:	*CrystEngComm*
Manuscript ID	CE-ART-04-2019-000599.R1
Article Type:	Paper
Date Submitted by the Author:	29-May-2019
Complete List of Authors:	Kimura, Fumiko; Kyoto University - Yoshida Campus, Graduate School of Energy Science; Kyoto University of Advanced Science, Nagamori Institute of Actuators Horii, Shigeru; Kyoto University Graduate School of Energy Science; Kyoto University of Advanced Science Arimoto, Itsuki; Kyoto University Graduate School of Energy Science Notsu, Daisuke; Kyoto University Graduate School of Energy Science Doi, Toshiya; Kyoto University - Yoshida Campus, Graduate School of Energy Science Wada, Masahisa; Kyoto University Graduate School of Agriculture Faculty of Agriculture; Kyung Hee University - Global Campus Kimura, Tsunehisa; Kyoto University Graduate School of Agriculture Faculty of Agriculture; Fukui University of Technology

ARTICLE

X-ray diffraction study on the orientation dynamics of biaxial microcrystals under static and rotating magnetic fields

Received 00th January 20xx,
Accepted 00th January 20xx

DOI: 10.1039/x0xx00000x

F. Kimura,*[a,b] S. Horii, [a,b] I. Arimoto, [a] D. Notsu, [a] T. Doi, [a] M. Wada,[c,d] and T. Kimura*[c,e]

The orientation of microcrystals of $DyBa_2Cu_3O_y$ (y~7) under static and rotating magnetic fields was studied. The suspension of the microcrystals was exposed to the static and rotating magnetic fields and their orientation process was monitored via *in-situ* X-ray diffraction (XRD) measurements. Under the static magnetic field, the orientation process was characterized by a single time constant, indicating that the microcrystal is close to be uniaxial. When the rotating magnetic field was applied, the two-dimensional XRD profile changed as a function of the rotation speed. The transition from the static profile to the rotating one was identified at a rotation speed ω_θ. At about $10 \times \omega_\theta$, the orientation of the hard-magnetization axis was completed.

Introduction

The orientation of nano- and microcrystals, whiskers, microfibers, etc. is an important element for improving the material properties of composites, green compacts for ceramics, and so forth. The physical, chemical, and biological properties can be highly improved by orientation. There are several means of orientations, including shears,[1] elongations,[2] epitaxial growth,[3, 4] self-organizations,[5-7] electric[8, 9] and magnetic[4, 10-19] fields, etc. Each of them has advantages and disadvantages and is used according to the material to be aligned and the purpose of the final product. It is possible to enhance the effect by combining them. Whiskers and microfibers can undergo uniaxial orientation the most because their physical properties and shapes are uniaxial. On the other hand, biaxial orientation (or three-dimensional orientation) is possible for biaxial nano- and microcrystals. Staines proposed a magnetic method to achieve the biaxial orientation of superconducting microcrystals to produce biaxially oriented green compacts.[20, 21]

Magnetic orientations can occur not only for ferromagnetic materials[22-24] but also for dia-[12, 16] and paramagnetic[18, 25] materials. In order to achieve biaxial orientation, the applied magnetic field should be time dependent (oscillating, rotating, etc.); the static magnetic field induces only the uniaxial orientation of the easy magnetic axis. The response of microcrystal suspension to the time-dependent magnetic field has three different time regimes. In the low-oscillation regime, the microcrystal responds synchronously to the applied oscillating field. When the oscillation speed increases, step-outs occur. If the oscillation is sufficiently high, the microcrystal cannot respond to the magnetic oscillation and is considered to have a time-averaged magnetic energy. It is known that the biaxial orientation can be achieved only in the high-oscillation regime.[26, 27]

The orientation dynamics of biaxial microcrystals are not well understood compared to those of uniaxial particles[15, 22, 28, 29]. We previously reported on the *in-situ* X-ray diffraction (XRD) observation of magnetic orientation of a biaxial microcrystal suspension under rotating magnetic fields. However, no detailed quantitative analyses were made[30]. In this paper, we studied the orientation dynamics of the biaxial crystal of $DyBa_2Cu_3O_y$ with y~7 (Dy123) under static and rotating magnetic fields using the XRD method. Dy123 is a superconducting material having high critical temperatures over liquid nitrogen temperature and can be used in practical applications such as superconducting bulk magnets and cables.

Results and discussion

Orientation dynamics under static magnetic field

The magnetic response of feeble magnetic materials (dia- and paramagnetic materials) is described by a magnetic susceptibility tensor. The magnetic susceptibility tensor of biaxial crystals (triclinic, monoclinic, and orthorhombic crystals) has three different principal values χ_1, χ_2, and χ_3, which correspond to the three principal axes. We define as $\chi_1 > \chi_2 > \chi_3$. For orthorhombic crystals, the crystallographic

[a] Graduate School of Energy Science, Kyoto University, Yoshida-Honmachi, Sakyo-ku, Kyoto 606-8501, Japan.
[b] Nagamori Institute of Actuators, Kyoto University of Advanced Science, Yamanouchi-Gotandacho, Ukyo-ku, Kyoto 615-8577, Japan. E-mail:Kimura.fumiko@kuas.ac.jp
[c] Division of Forestry and Biomaterials, Kyoto University, Kitashirakawa, Sakyo-ku, Kyoto 606-8502, Japan. E-mail:tkimura@kais.kyoto-u.ac.jp
[d] Department of Plant & Environmental New Resources, College of Life Sciences, Kyung Hee University, 1732 Deogyeong-daero, Giheung-gu, Yongin-si, Gyeonggi-do 446-701, Republic of Korea.
[e] Fukui University of Technology, 3-6-1 Gakuen, Fukui 910-8505, Japan
† Footnotes relating to the title and/or authors should appear here.
Electronic Supplementary Information (ESI) available: [details of any supplementary information available should be included here]. See DOI: 10.1039/x0xx00000x

a, *b*, and *c* axes and principal χ_1, χ_2, and χ_3 axes are in a

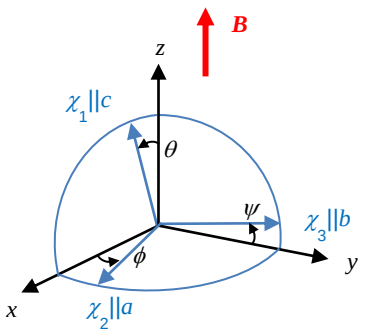

Fig. 1 Relationship between the χ_1, χ_2, and χ_3 axes and the crystallographic *a*, *b*, and *c* axes of the Dy123 crystal. Definition of the Euler angles ϕ, θ, and ψ that relate to the $\chi_1\chi_2\chi_3$ coordinates to the laboratory *xyz* coordinates. Here, two coordinate systems are assumed to be close. In such a condition, the angles ϕ, θ, and ψ are regarded as rotation angles about the *z*-, *y*-, and *x*-axes, respectively. A static magnetic field ***B*** is applied in the *z*-direction.

parallel relationship.[31] The crystal of Dy123 is orthorhombic (*a*=3.8244, *b*=3.8890, *c*=11.6885 Å)[32], and $a \| \chi_2$, $b \| \chi_3$, and $c \| \chi_1$ (Fig. 1). For uniaxial crystals, including trigonal, tetragonal, and hexagonal crystals, χ_2 is equal to χ_1 or χ_3. If $\chi_2 = \chi_1$, the χ_3 axis is the primary axis, and if χ_2=χ_3, the χ_1 axis is the primary axis.

The magnetic orientation of a single piece of microcrystal suspended in a viscous medium is described by the equation of balance between the magnetic and hydrodynamic torques. Under a static magnetic field ***B***, a magnetic torque is exerted to align the χ_1 axis in the direction of ***B***. If a microcrystal is magnetically uniaxial, the direction of its primary axis with respect to the magnetic field is described by an angle α. The temporal change of α is described by the following equation,[11, 22, 28, 29, 33] assuming that the shape of the microcrystal is spherical:

$$\tan\alpha = (\tan\alpha_0)\exp(-t/\tau_a), \quad (1)$$

where τ_a is the orientation time defined by

$$\tau_a = 6\mu_0\eta/(\chi_a B^2). \quad (2)$$

Here, μ_0, η, and B are the magnetic permeability of the vacuum, the viscosity of the suspension, and the intensity of the magnetic field, respectively. We define as $\chi_a = \chi_\parallel - \chi_\perp$, where the parallel and perpendicular symbols indicate the direction of the primary axis and the direction perpendicular to it, respectively.

If the microcrystal is biaxial, we need three angles to identify the orientation of the $\chi_1\chi_2\chi_3$ coordinates relative to the laboratory *xyz* coordinates. For this purpose, the Euler angles ϕ, θ, and ψ are usually used. By solving the equation of the torque balance, we express ϕ, θ, and ψ as a function of time.[34] However, the solution to this equation can only be obtained numerically. In this paper, we extend analytical expressions, eqs. (1) and (2), obtained for uniaxial crystals to describing the orientation process of a biaxial crystal. In Fig. 1, the definition of the Euler angles is shown, where ϕ, θ, and ψ are assumed to be small. We assume that the temporal change for these angles is expressed by eq. (1), where α represents ϕ, θ, and ψ. Accordingly, we have three time constants: the time constant τ_a in eq. (2) are replaced with τ_ϕ, τ_θ and τ_ψ. These are inversely proportional to $\chi_2-\chi_3$, $\chi_1-\chi_2$, and $\chi_1-\chi_3$, respectively. By definition, $\tau_\phi, \tau_\theta > \tau_\psi$. The time constants τ_ϕ, τ_θ and τ_ψ are closely related to the rotation about the χ_1, χ_3, and χ_2 axes, respectively.

The use of a distribution function is better suited when the orientation behavior is studied by XRD. Let us consider a distribution function $P(\alpha, t{:}\,\tau_a)$ for uniaxial microcrystals exposed to a static magnetic field. Here, α is the angle between the $\chi_\parallel$ axis and the magnetic field, and τ_a is defined by eq. (2). $P(\alpha, t{:}\,\tau_a)$ is proportional to the population of the microcrystals having the angle α at time t after the onset of the magnetic field. In the initial state, we assume $P(\alpha, 0{:}\,\tau_a) = \text{const}$. Upon exposure to the magnetic field, the individual microcrystals start to orient according to eq. (1) with their own initial α_0 values. The distribution function at time t is expressed by[11, 35]

$$P(\alpha, t{:}\,\tau_a) = \frac{e^{\frac{2t}{\tau_a}}\sec^3\alpha}{4\pi\left(1+e^{\frac{2t}{\tau_a}}\tan^2\alpha\right)^{\frac{3}{2}}} \quad (3)$$

This expression is more convenient than eq. (1) because the change in the α of a single microcrystal is difficult to measure, while the distribution $P(\alpha, t{:}\,\tau_a)$ is easily determined experimentally through the XRD azimuthal profile.

We extend eq. (3) to biaxial microcrystals. We need three distribution functions $P(\theta, t{:}\,\tau_\theta)$, $P(\psi, t{:}\,\tau_\psi)$, and $P(\phi, t{:}\,\tau_\phi)$, corresponding to three angles, θ, ψ, and ϕ, respectively. Since the reciprocal vectors are embedded in the magnetic $\chi_1\chi_2\chi_3$ frame, their orientation is driven by the magnetic orientation of the $\chi_1\chi_2\chi_3$ frame. The distribution function can be approximately expressed by the sum of two distribution functions:

$$P(\beta-\beta_0, t{:}\,\tau_\theta, \tau_\psi) = K_\theta P(\beta-\beta_0, t{:}\,\tau_\theta) + K_\psi P(\beta-\beta_0, t{:}\,\tau_\psi), \quad (4)$$

where β is the X-ray azimuthal β-scan angle for an arbitrary reciprocal vector and β_0 is the location of the peak center. Here, K_θ and K_ψ are constants. We assume that under a static magnetic field the angle ϕ does not appear as long as χ_1 is oriented closely parallel to the magnetic field, because there is freedom of rotation about the magnetic field.

Figure 2 shows two two-dimensional XRD profiles obtained at t =1 and 50 min for Dy123 microcrystals suspended in PEG solution. It was found that the initial broad arcs become sharp when magnetic orientation proceeds. Here we focus on the diffraction spot from the reciprocal vectors {013} and {103}, enclosed in the figure because their intensities are high enough for the analyses. The reciprocal vectors {013} and {103} are located in the $\chi_1\chi_3$ and $\chi_1\chi_2$ planes, respectively, and hence their motions are related to τ_ψ and τ_θ, respectively.

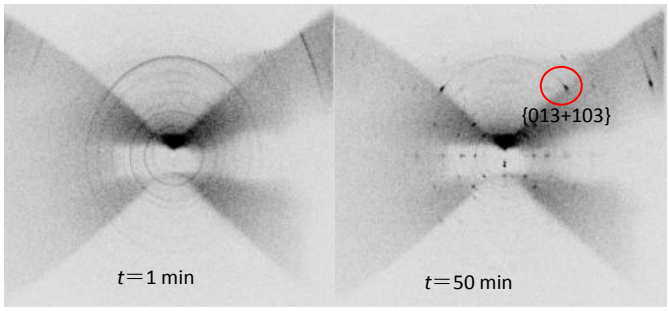

Fig. 2 Two dimensional XRD profiles from a PEG suspension of the Dy123 microcrystals measured at 1 and 50 min after the start of applying a vertical magnetic field (~1 T). A spot encircled in red is originating from {013} and {103} diffractions.

Because $a \cong b$, these two diffractions appear almost at the same position in the two-dimensional profile. In Fig. 3, the azimuthal β-scans for a mixture of {013} and {103} diffractions are show for t =9.0, 11.5, 14.0, and 16.5 min. The peaks sharpen with time. These peak profiles are fitted to eq. (4), where we put $\tau_\theta = \tau_\psi$= 13 min. Good fitting is obtained though the peaks should be fitted using two different values of τ_θ and τ_ψ. This good fitting might indicate that the values of χ_2 and χ_3 are close because $\chi_1-\chi_2$ and $\chi_1-\chi_3$ are proportional to τ_θ and τ_ψ, respectively. This observation is partially supported by the fact that the Dy123 microcrystal has a twin structure[36, 37] originating from the tetragonal-orthorhombic transition: the (110) plane is shared in a such a manner that the two crystallographic $c(\| \chi_1)$ axes are antiparallel to each other. Moreover, they showed that the twins formed a band shape with a width of 50 to 200 nm by the TEM observation. Therefore, the Dy123 microcrystal is regarded close to uniaxial with the χ_1 axis being the primary axis.

Orientation dynamics under rotating magnetic field

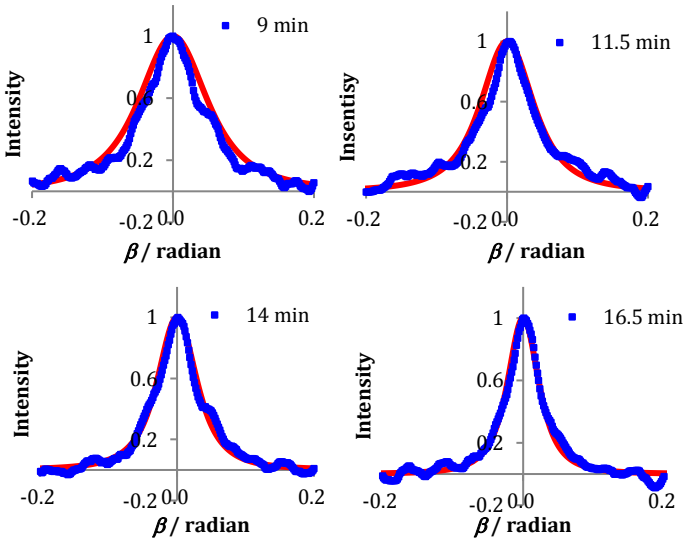

Fig. 3 Azimuthal β scans of the XRD spot for a mixture of {013} and {103} measured at t =9.0, 11.5, 14.0, and 16.5 min. Peak profiles are fitted to eq. (3) with $\tau_\theta = \tau_\psi$= 13 min.

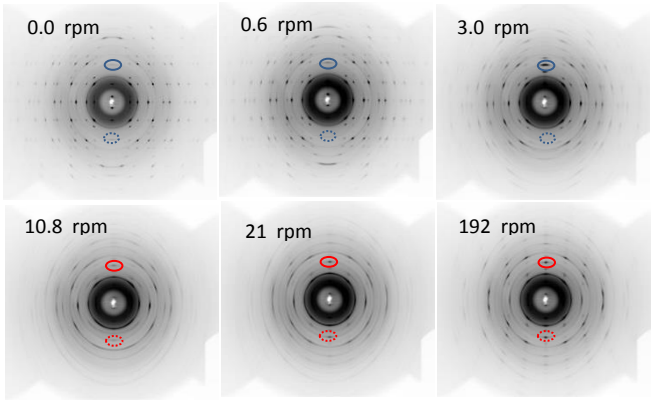

Fig. 4 A series of XRD profiles of Dy123 microcrystal suspension as a function of the sample rotation speed ω. ω =0 and 192 rpm correspond to static and rotating orientations, respectively. Diffraction spots in blue and red ellipses correspond to {006} and a mixture of {006} and {200}, respectively.

The χ_1 axis ($\chi_\|$ axis) of the uniaxial crystal aligns in the direction of the applied static magnetic field. On the other hand, if the magnetic field is rotating in a plane, for example in the *xz* plane, the motion of the χ_1 axis is different.[22, 28, 29, 33] If the rotation speed ω is slow, the χ_1 axis follows the magnetic rotation with a phase delay and its direction is not settled. This occurs when $\omega\tau_a < 1/2$, where τ_a is defined by eq. (2), and is referred to as synchronous rotation regime (SRR). If $\omega\tau_a > 1/2$, the χ_1 axis follows the magnetic rotation, but with occasional step-outs, which is referred to as asynchronous rotation regime (ARR). If $\omega\tau_a \to \infty$, the χ_1 axis cannot respond to the magnetic rotation. This regime is referred to as rapid rotation regime (RRR). For the biaxial orientation of biaxial crystals, the RRR condition is required.

The orientation dynamics of biaxial crystals in a rotating magnetic field are different from those of uniaxial crystals because their three susceptibility values are not the same. As discussed earlier, there should be three time constants, τ_ϕ, τ_θ and τ_ψ instead of a single τ_a. These time constants can be related to the critical rotation speeds defined by $\omega_\phi = 1/(2\tau_\phi)$, $\omega_\theta = 1/(2\tau_\theta)$, and $\omega_\psi = 1/(2\tau_\psi)$. These critical speeds might be related to the onset of the rotation about the χ_1, χ_3, and χ_2 axes, respectively.

Figure 4 shows a series of two dimensional XRD profiles of the suspension of Dy123 microcrystals as a function of the rotational speed ω. The X-ray beam was impinged from the *x*-axis, and the suspension was rotated about the *y*-axis (see Fig. 1). So far we have assumed that a magnetic field rotating in a plane, for example in the *xz*-plane, is applied to a suspension. However, in actual experiments, it is difficult to combine the magnetic field rotation and the *in-situ* X-ray diffraction measurement. Therefore, we instead rotate the suspension in a static magnetic field. This gives the same effect as rotating magnetic field. It should be noted that the viscosity of the suspension used for the rotating measurement is far lower than that used for the static measurement. Therefore, the equilibrium is achieved during each sweep of ω. The profile at $\omega = 0$ is characteristic of a static orientation of the orthorhombic system: horizontally layered lines are

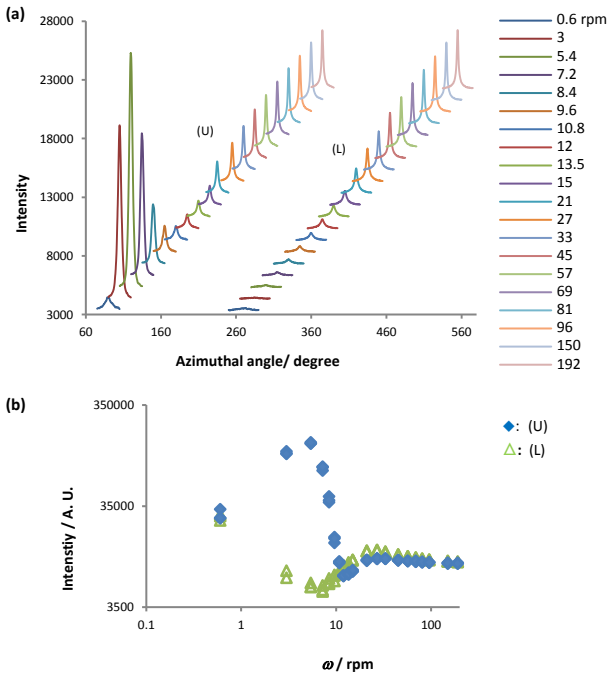

Fig. 5 Diffraction data obtained from Dy123 suspension. (a) Change in the intensity against the azimuthal angle. (b) Change in the intensity of only {006} or the sum of {006} and {200} diffractions (encircled in Fig. 4) as a function of rotation speed ω. Filled and open symbols correspond to the diffractions appearing at upper and lower semispheres, respectively.

observed.[38] The profile at $\omega = 192$ rpm exhibits a diffraction pattern characteristic of a rotational orientation of the orthorhombic system: vertically layered lines are observed.[38]

The profile changes gradually from a static one to a rotational one. Let us focus on the spots in Fig. 4 enclosed by solid and broken circles located in the upper (U) and lower (L) hemispheres, respectively. We denote the reciprocal vectors that give rise to the spots in (U) and (L) as ***G***(U) and ***G***(L), respectively. When $\omega \leq 3$ rpm, ***G***(U) and ***G***(L) are composed of the reciprocal vector {006} (indicated by blue ellipses), while when $\omega \geq 10.8$, they are composed of the reciprocal vectors {006} and {200} (indicated by red ellipses); they appear in proximity because the lattice length c is almost exactly three times as large as the lattice length a, and the reciprocal vectors, {006} and {200}, are on the χ_1 and χ_2 axes, respectively (see Fig. 1).

In Fig. 5(a), a stuck plot of the azimuthal peaks for the (U) and (L) spots in Fig. 4 is shown as a function of ω. These peaks were curve-fitted using the Lorentz function, and peak areas were integrated to obtain the peak intensity. In Fig. 5(b), the peak intensity is shown as a function of ω. A characteristic feature of Fig. 5(b) is that at low ω values the intensity of the spot (U) increases, while that of the spot (L) decreases. Then, at $\omega \cong 10$ rpm, both intensities become identical. The intensities finally reach a constant value at around 100 rpm.

The above observation is interpreted as follows. Figure 6 shows the reciprocal sphere and its line of intersection (LI) with the Ewald sphere. The impinged X-ray is diffracted by reciprocal vectors located on the LI. Under the static magnetic

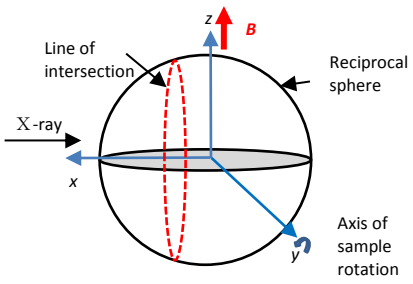

Fig. 6 *In-situ* XRD observation of a rotating microcrystalline suspension. The suspension is rotated about the *y*-axis at a speed of ω under magnetic field ***B*** applied in the *z* direction. The X-ray is impinged from the *x* direction and diffracted by reciprocal vectors located on the line of intersection (LI) (broken red line) formed by the reciprocal sphere and the Ewald sphere (not shown). The χ_1 axis is in the *xz* plane and the χ_2 and χ_3 axes are distributed in the plane perpendicular to the χ_1 axis.

field applied to the *z*-axis, ***G***(U) and ***G***(L) direct to the *z* and –*z* directions, respectively. When the rotation speed ω is lower than $\omega_\theta \cong 1/(2\tau_\theta)$ (the SRR condition) ***G***(U) deviates from the *z*-axis by an angle δ toward the LI. This deviation increases with an increase in ω. As a result, the XRD intensity increases with an increase in ω until ***G***(U) comes across with the LI. Then, with a further increase in ω, ***G***(U) moves away from the LI, resulting in a decrease in the XRD intensity. On the other hand, ***G***(L) moves away from the LI at SRR, resulting in a decrease in the XRD intensity. ***G***(U) and ***G***(L) are composed of diffractions by {006} ($\|\chi_1$axis) in the case of SRR. When $\omega > \omega_\theta$, both ***G***(U) and ***G***(L) start to rotate synchronously with the rotation of the suspension with occasional step-outs. Because the X-ray exposure time was 3.0 min, the sample underwent sufficient revolutions during the X-ray measurement. At this stage, ***G***(U) and ***G***(L) have an equal chance to come across the LI, giving rise to the same intensities. Therefore, we conclude that ω_θ is located at around 10 rpm in Fig. 5(b). This indicates $\tau_\theta \cong 0.5$ s. The suspension used in the measurement under the static magnetic field was so viscous that the viscosity was not measured. However, τ_θ (static)/ τ_θ (rotating) $\cong 13 \times 60/0.5 = 1{,}560$, indicating that $\eta(\text{static}) = 2 \times \eta(\text{rotating}) \times 1{,}560 = 2 \times 12 \times 1{,}560 = 37{,}440$ Pa s, where the factor 2 is inserted because the effective field intensity for the rotating field is $1/\sqrt{2}$ of the static field. Around $\omega =$ ca. 100 rpm, the intensities of ***G***(U) and ***G***(L) become to coincide. This indicates that $10 \times \omega_\theta$ is sufficient to achieve the RRR condition. In this experiment, only ω_θ was clearly identified. The time constant τ_θ is related to ω_θ via the relationship $\tau_\theta = 1/(2\omega_\theta)$ and is relevant to the rotation about the χ_3 axis. The driving force that brings the χ_1 axis to the direction of the magnetic field is proportional to the magnetic anisotropy $\chi_1 - \chi_2$. The larger is this driving force (the shorter is τ_θ), the stronger is the tendency of the χ_1 axis to stay with the magnetic field. When the rotation speed exceeds $\omega_\theta = 1/(2\tau_\theta)$, the χ_1 axis starts to rotate in synchronization with the sample rotation. The physical meaning of ω_ϕ and ω_ψ in relation to the XRD measurement are no clear at present.

Experimental

Preparation of Dy123 powder and pulverization

Polycrystals of Dy123 were synthesized by standard solid-state reaction in air.[37] The starting materials, Dy_2O_3, $BaCO_3$, and CuO, were weighed in a molar ratio of 1:2:3 and ground thoroughly in ethanol. The mixed powders were calcined twice at 860°C and 880°C with intermediate grindings. They were then pelletized and sintered for 24 h at 960°C to control grain growth during the sintering process. The obtained Dy123 pellets were post-annealed in flowing oxygen gas, crushed in an agate mortar, and then ball-milled for 30 h.

Preparation of uniaxially oriented suspension and *in-situ* X-ray measurements

Dy123 microcrystals were suspended in a 10 % polyethylene glycol (PEG, product of Wako Pure Chemical Corporation, Polyethylene Glycol 4,000,000 with average molecular weight =3,600,000-4,000,000) aqueous solution having a concentration of ca. 10 wt.% Dy123, which was used for the orientation dynamics under static magnetic field. The suspension was so viscous that a viscosity measurement was not performed. Dy123 microcrystals were suspended in a UV curable monomer (XVL14, a modified acrylate supplied by Kyoritsu Chemical & Co., Ltd., viscosity 12 Pa s) having a concentration of ca. 10 wt.% Dy123 for the study of orientation dynamics under rotating magnetic field. The viscosity of the suspensions was much lower than that of the suspension used for the measurement under static magnetic field. This low viscosity ensured that the alignment was achieved quickly when the rotation speed changed. *In-situ* XRD measurements were performed at room temperature using CuKα for the measurement under static magnetic field and Mokα for the measurement under rotating magnetic field, with a two-dimensional detector (Rigaku Rapid II). The crystal-to-detector distance was 14.7 mm.

Data processing

Using 2D Data Processing software (2DP, product of Rigaku Corporation), the diffraction intensities were integrated at 2ϑ = ca. 32.5° (for the study of orientation dynamics under the static magnetic field) and 21° (for the study of the orientation dynamics under the rotating magnetic field) with width of 1° in 0.1° steps to obtain the azimuthal profile. The diffraction peaks were fitted using the Lorentz function with IGOR software to determine the half width.

Conclusions

The orientation process of suspensions of Dy123 microcrystals under static and rotating magnetic fields was studied by means of XRD measurements. The magnetic orientation of the Dy123 crystal, being biaxial (orthorhombic), might in principle be governed by three time constants τ_ϕ, τ_θ and τ_ψ, which are inversely proportional to $\chi_2-\chi_3$, $\chi_1-\chi_2$, and $\chi_1-\chi_3$, respectively. Under the static magnetic field, the orientation process is assumed to be driven by the rotation process characterized by τ_θ and τ_ψ. However, the XRD result exhibited only one time constant, indicating that $\tau_\theta \cong \tau_\psi$. This indicated that the Dy123 microcrystal is close to uniaxial where $\chi_2 \cong \chi_3$, which can be attributed to the twin structure of this microcrystal. Under the rotating magnetic field, the critical rotation speeds $\omega_\phi = 1/(2\tau_\phi)$, $\omega_\theta = 1/(2\tau_\theta)$, and $\omega_\psi = 1/(2\tau_\psi)$ can be formally introduced. In the XRD measurement, only ω_θ was identified. In order to achieve the RRR condition, the rotation speed of ca. $10 \times \omega_\theta$ was sufficient.

Conflicts of interest

There are no conflicts to declare.

Acknowledgements

This work was partly supported by the Adaptable and Seamless Technology Transfer Program through Target-driven R&D (A-STEP), the Japan Science and Technology Agency (JST) and JSPS KAKENHI Grant Number JP17H03235.

References

1. Y. Nishiyama, S. Kuga, M. Wada and T. Okano, *Macromolecules* 1997, **30**, 6395-6397.
2. C. Luap, C. Müller, T. Schweizer and D. C. Venerus, *Rheologica Acta*, 2005, **45**, 83-91.
3. R. Xu, R. Gao, S. E. Reyes-Lillo, S. Saremi, Y. Dong, H. Lu, Z. Chen, X. Lu, Y. Qi, S.-L. Hsu, A. R. Damodaran, H. Zhou, J. B. Neaton and L. W. Martin, *ACS Nano*, 2018, **12**, 8.
4. S. Teranishi, R. Kusumi, F. Kimura, T. Kimura, K. Aburaya and M. Maeyama, *Chemistry Letters*, 2017, **46**, 3.
5. M. Mashkour, T. Kimura, F. Kimura, M. Mashkour and M. Tajvidi, *Biomacromolecules*, 2014, **15**, 60−65.
6. Y. Zhao, G. Cavallaro and Y. Lvov, *J Colloid Interface Sci*, 2015, **440**, 68-77.
7. H. Jung, D. Hwang, E. Kim, B.-J. Kim, W. B. Lee, J. E. Poelma, J. Kim, C. J. Hawker, J. Huh, D. Y. Ryu and J. Bang, *ACS Nano*, 2011, **5**, 10.
8. Bianca M. I. van der Zande, Ger J. M. Koper and H. N. W. Lekkerkerker, *J. Phys. Chem. B* 1999, **103**, 5754-5760.
9. D. Bordel, J. L. Putaux and L. Heux, *Langmuir*, 2006, **22**, 4899-4901.
10. J. Torbet, J.-M. Freyssinet and G. Hudry-Clergeon, *Nature*, 1981, **289**, 91.
11. J. S. Moore and S. I. Stupp, *Macromolecules*, 1987, **20**, 282-293.
12. J. M. Freyssinet, J. Torbet, G. Hudry-Clergeon and G. Maret, *Proc Natl Acad Sci U S A*, 1983, **80**, 1616-1620.
13. J. Sugiyama, H. Chanzy and G. Maret, *Macromolecules*, 1992, **25**, 4232-4234.
14. M. Fujiwara, M. Fukui and Y. Tanimoto, *The Journal of Physical Chemistry B*, 1999, **103**, 2627-2630.
15. T. Kimura, M. Yamato, W. Koshimizu, M. Koike and T. Kawai, *Langmuir*, 2000, **16**, 858-861.
16. T. Kimura, *Polymer Journal*, 2003, **35**, 823.
17. T. Kimura, F. Kimura and M. Yoshino, *Langmuir*, 2006, **22**, 3464-3466.

18. A. Ishihara, S. Horii, T. Uchikoshi, T. S. Suzuki, Y. Sakka, H. Ogino, J.-i. Shimoyama and K. Kishio, *Applied Physics Express*, 2008, **1**, 031701.
19. Y. Dong, F. Liu, W. Yang, J. Zhu, J. Yu and Y. Hou, *CrystEngComm*, 2014, **16**, 4.
20. M. Staines, *New Zealand Pat.*319724, 1995.
21. J.-Y. Genoud, M. Staines, A. Mawdsley, V. Manojlovic and W. Quinton, *Superconductor Science and Technology*, 1999, **12**, 663.
22. M. Tan, H. Song, P. Dhagat, A. Jander and T. W. Walker, *Physics of Fluids*, 2016, **28**, 062004.
23. S. Yamamoto, T. Terai, T. Fukuda, K. Sato, T. Kakeshita, S. Horii, M. Ito and M. Yonemura, *Journal of Magnetism and Magnetic Materials*, 2018, **451**, 1-4.
24. N. Hiratsuka, K. Kakizaki and M. Sugimoto, *Le Journal de Physique IV*, 1997, **07**, C1-69-C61-70.
25. N. Nakatsuka, H. Yasuda, T. Nagira and M. Yoshiya, 2009.
26. F. Kimura and T. Kimura, *CrystEngComm*, 2018, **20**, 861-872.
27. M. Yamaguchi, S. Ozawa, I. Yamamoto and T. Kimura, *Japanese Journal of Applied Physics*, 2012, **52**, 013003.
28. J. Akiyama, H. Asano, K. Iwai and S. Asai, *Materials transactions*, 2008, **49**, 787-791.
29. T. Kimura, *Japanese Journal of Applied Physics* 2009, **48**, 020217.
30. K. Matsumoto, F. Kimura, S. Tsukui and T. Kimura, *Crystal Growth & Design*, 2011, **11**, 945-948.
31. J. F. Nye, *Physical properties of crystals: their representation by tensors and matrices*, Oxford university press, 1985.
32. G. D. Chryssikos, E. I. Kamitsos, J. A. Kapoutsis, A. P. Patsis, V. Psycharis, A. Koufoudakis, C. Mitros, G. Kallias, E. Gamari-Seale and D. Niarchos, *Physica C* 1995, **254**, 44-62.
33. T. Kimura, M. Yoshino, T. Yamane, M. Yamato and M. Tobita, *Langmuir* 2004, **20**, 5669-5672.
34. S. Tsukui and T. Kimura, *Japanese Journal of Applied Physics* 2012, **51**, 057301.
35. T. Kimura, H. Sata and E. Ito, *Polymer Journal*, 1998, **30**, 455-462.
36. Z. Hiroi, M. Takano, Y. Takeda, R. Kanno and Y. Bando, *Japanese Journal of Applied Physics*, 1988, **27**, 4.
37. S. Horii, T. Nishioka, I. Arimoto, S. Fujioka and T. Doi, *Supercond. Sci. Technol.*, 2016, **29**, 125007 (125006pp).
38. K. Matsumoto, F. Kimura, G. Song, S. Yamane, H. Kikuchi, T. Tanaka, S. Higuchi, N. Kitamura and T. Kimura, *Cryst. Growth Des.* , 2014, **14**, 6486−6491.

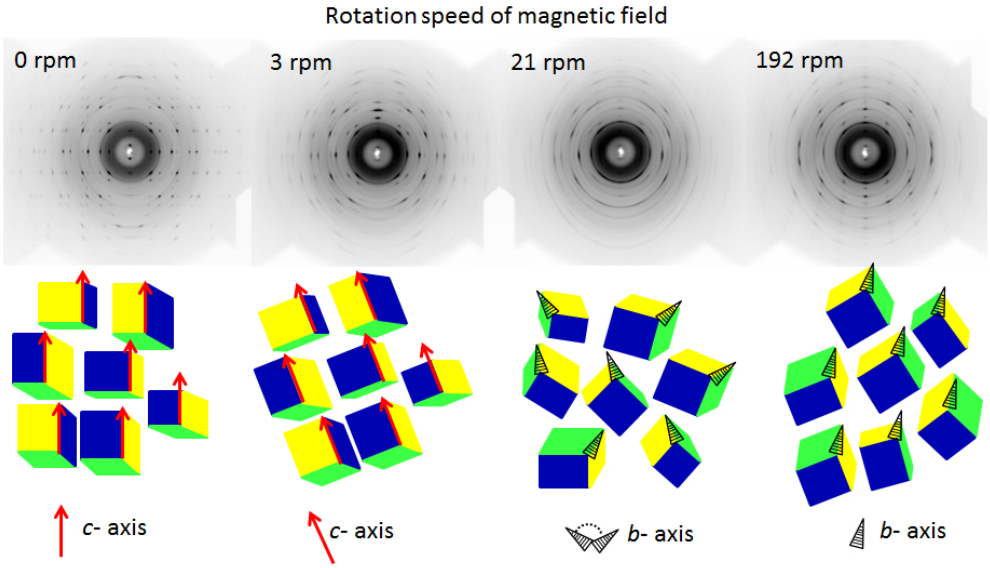
Rotation speed of magnetic field
0 rpm
3 rpm
21 rpm
192 rpm
c- axis
c- axis
b- axis
b- axis